Cell Death and Differentiation (2002) 9, 27–39

www.nature.com/cdd

Hyperphosphorylation of histone H2A.X and dephosphorylation of histone H1 subtypes in the course of apoptosis

H Talasz*,[1], W Helliger[1], B Sarg[1], PL Debbage[2], B Puschendorf[1] and H Lindner[1]

[1] Institute of Medical Chemistry and Biochemistry, University of Innsbruck, Innsbruck, Austria
[2] Institute of Anatomy and Histology, University of Innsbruck, Innsbruck, Austria
* Corresponding author: H Talasz, Institute of Medical Chemistry and Biochemistry, Fritz-Pregl-Str. 3, A-6020 Innsbruck, Austria.
Tel: +43 512 507 3522; Fax: +43 512 507 2876;
E-mail: Heribert.Talasz@uibk.ac.at.

Received 13.12.00; revised 21.5.01; accepted 28.6.01
Edited by S Nagata

Abstract

Chromatin condensation paralleled by DNA fragmentation is one of the most important nuclear events occurring during apoptosis. Histone modifications, and in particular phosphorylation, have been suggested to affect chromatin function and structure during both cell cycle and cell death. We report here that phosphate incorporation into all H1 subtypes decreased rapidly after induction of apoptosis, evidently causing a strong reduction in phosphorylated forms of main H1 histone subtypes. H1 dephosphorylation is accompanied by chromatin condensation preceding the onset of typical chromatin oligonucleosomal fragmentation, whereas H2A.X hyperphosphorylation is strongly correlated to apoptotic chromatin fragmentation. Using various kinase inhibitors we were able to exclude some of the possible kinases which can be involved directly or indirectly in phosphorylation of histone H2A.X. Neither DNA-dependent protein kinase, protein kinase A, protein kinase G, nor the kinases driven by the mitogen-activated protein kinase (MAP) pathway appear to be responsible for H2A.X phosphorylation. The protein kinase C activator phorbol 12-myristate 13-acetate (PMA), however, markedly reduced the induction of apoptosis in TNFα-treated cells with a simultaneous change in the phosphorylation pattern of histone H2A.X. Hyperphosphorylation of H2A.X in apoptotic cells depends indirectly on activation of caspases and nuclear scaffold proteases as shown in zVAD-(OMe)-fmk- or zAPF-cmk-treated cells, whereas the dephosphorylation of H1 subtypes seems to be influenced solely by caspase inhibitors. Together, these results illustrate that H1 dephosphorylation and H2A.X hyperphosphorylation are necessary steps on the apoptotic pathway. *Cell Death and Differentiation* (2002) **9,** 27–39. DOI: 10.1038/sj/cdd/4400925

Keywords: apoptosis; DNA fragmentation; histones; phosphorylation

Abbreviations: PARP, poly(ADP-ribose) polymerase; PMA, phorbol 12-myristate 13-acetate; MAP kinase, mitogen-activated protein kinase; MEK, mitogen-activated protein kinase kinase; DNA-PK, DNA-protein kinase; PI3-K, phosphatidylinositol 3-kinase; AUT, acetic acid-urea-Triton X-100; AU, acetic acid-urea; PAGE, polyacrylamide gel electrophoresis

Introduction

Apoptosis is an active form of cellular suicide with many well-defined morphological and biochemical features. The process of apoptosis is initiated by external inducers or treatments including UV- or γ-irradiation, heat shock, oxidative stress, viral infection, glucocorticoids, soluble or membrane-bound cytokines like TNF or Fas/Apo-1 (CD95) ligand and many others. The different pathways of these various agents then presumably converge to form an apoptotic pathway common to all cells. Whereas the early stages of apoptosis are biochemically well characterized, the biochemical basis for the nuclear events is still unclear. The morphological nuclear events of apoptosis are chromatin condensation, DNA fragmentation to domain-sized fragments (200–300 kb and 30–50 kb) and finally to nucleosomal-sized fragments (180–200 bp).[1,2] An apoptosis-specific caspase-activated DNase termed CAD or DFF40 seems to be responsible for internucleosomal DNA cleavage[3,4] and chromatin condensation as well as formation of apoptotic bodies.[5] It is, however, not fully understood whether apoptotic fragmentation of chromatin occurs randomly or whether specific modifications of chromatin-associated proteins determine preferential cleavage. Little is known about the mechanism or the biological function of chromatin condensation and internucleosomal DNA cleavage after apoptosis induction. The late stages of the apoptotic process typically involve cleavage of specific target proteins like lamin,[6] actin[7] or poly(ADP-ribose) polymerase.[8,9] Several protein kinases like DNA-dependent protein kinase,[10] or protein kinase Cδ[11] have been proposed as being involved in apoptosis. Phosphorylation and dephosphorylation of proteins are essential control elements in cell cycle progression and are also involved in structural changes in chromatin. Histone phosphorylation at specific sites, in particular, has been shown to be involved in structural changes in chromatin during the cell cycle.[12] The cdc 2/H1 kinase-dependent phosphorylation of H1 histones during the cell cycle is a dynamic process with a phosphorylation maximum during mitosis.[13] Whereas H2A histones are constantly phosphorylated, phosphorylation of H4 and H2B histones is negligible throughout the cell cycle. Histone H3 phosphorylation, in particular, appears to be essential for proper mitotic chromosome condensation and segregation,[14,15] but was also shown to be involved in premature

chromosome condensation. In apoptotic cells, however, with chromatin condensation as an essential nuclear event, histone H3 phosphorylation at mitosis-associated sites does not occur, although H2B phosphorylation at the specific serine 32 was associated with DNA fragmentation in mammalian apoptotic cells.[16]

Since histones and their modified forms play a fundamental role in chromatin structure, the aim of this study was to investigate the phosphorylation events of histone proteins during apoptosis and to correlate them to morphological changes occurring in apoptotic cells. Using TNFα or agonistic anti-Fas antibody, NIH 3T3 cells are killed by both activating stimuli in a characteristically apoptotic fashion, causing phosphatidylserine externalization, and chromatin condensation.[17] Our results show that both TNFα- and CD95-mediated cell killing results in nearly the same change in the phosphorylation pattern of histone proteins. During induction of apoptosis but before initiation of nucleosomal fragmentation H1 histones became rapidly dephosphorylated, which was accompanied by condensation of chromatin. Parallel to nucleosomal chromatin fragmentation histone H2A.X became more highly phosphorylated with increasing amounts of mono- and diphosphorylated forms in the case of TNFα- or anti-Fas-induced apoptosis and mono- to triphosphorylated forms in cantharidin-treated cells.

Results

Morphological changes after apoptosis induction in NIH 3T3 cells

Figure 1A shows the morphological features of nuclear chromatin in NIH 3T3 cells untreated (Figure 1A, Control) or treated with TNFα in the presence of cycloheximide for 1 to 8 h (Figure 1A). Treatment with either cycloheximide, a potent protein synthesis inhibitor, or TNFα alone induces apoptosis after only 48 to 72 h. With the combination of TNFα and cycloheximide the induction of apoptosis in NIH 3T3 fibroblasts can be substantially accelerated. Nuclear fragmentation and condensation of the chromatin at the nuclear membrane are visible in fluorescence microscopy in some cells after 3 h of treatment. The number of cells with apoptotic features increased during the next 5 h of treatment, reaching about 80% of apoptotic cells after 8 h (Figure 1A). Figure 1B shows gel electrophoresis of DNA from cells after induction of apoptosis. One hour of TNFα treatment resulted in a small but clearly visible shift in high molecular weight DNA (Figure 1B, lane 2), whereas after 2 h (Figure 1B, lane 3) a DNA ladder started to become visible and was prominent after 8 h of TNFα treatment (Figure 1B, lane 8). Electron microscopy was used to demonstrate the morphological changes in NIH 3T3 cells after treatment with TNFα in greater detail (Figure 2). Control cells appeared normal, with typical distributions of nuclear heterochromatin, and with a smooth cell surface (Figure 2A). One hour after incubation with TNFα, many cells exhibited pronounced blebbing. A thicker layer of condensed chromatin is present at most points of the nuclear membrane, sparing the nuclear pores (small arrow). (Figure 2B,H). By 2 h the blebbing was accompanied by further condensation of the

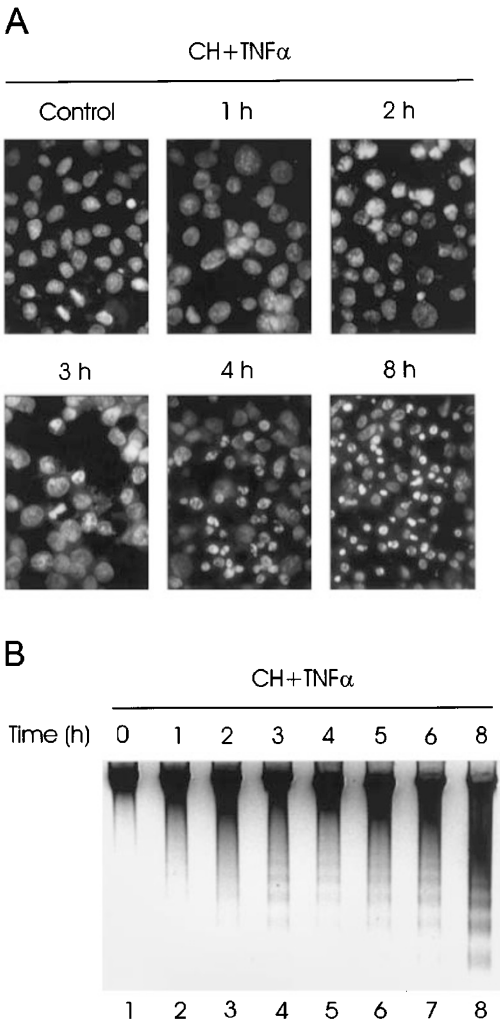

Figure 1 Apoptosis induction after treatment with TNFα. (**A**) Fluorescence microscopy of NIH 3T3 cells stained with Hoechst 33258. The panels correspond to untreated (control), 1, 2, 3, 4 and 8 h TNFα-treated cells, respectively. TNFα was in the presence of cycloheximide. (**B**) DNA of TNFα-treated apoptotic NIH 3T3 cells was separated on 2% agarose gel. Lanes 1 to 8 correspond to 0, 1, 2, 3, 4, 5, 6 and 8 h of TNFα treatment in the presence of cycloheximide (CH+TNFα)

chromatin, which had begun to accumulate at the nuclear membrane (Figure 2C). Three to four hours after incubation with TNFα, condensation of chromatin at the nuclear membrane was conspicuous, and almost all the mitochondria were disrupted (Figures 2D,E). By 6 h, many cells lacked integral cell membranes (Figure 2F), and the proportion of cells in this condition increased until the final electron microscopic observation at 8 h. The condensation of chromatin and its accumulation at the nuclear membrane is shown in greater detail in Figure 2G–I.

Phosphorylation of histones in NIH 3T3 cells undergoing TNFα-induced apoptosis

To investigate the phosphorylation levels of histone variants after induction of apoptosis NIH 3T3 fibroblasts were labeled

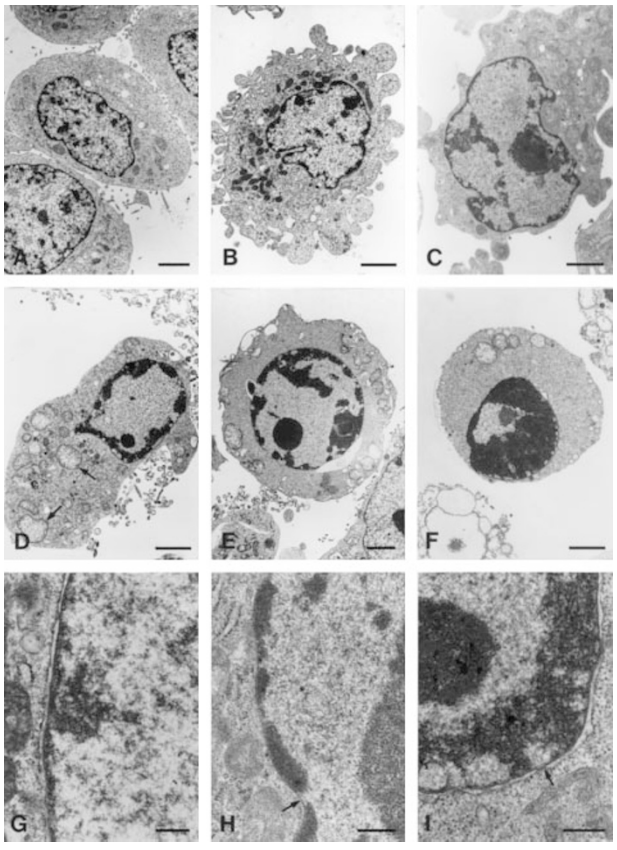

Figure 2 Electron micrographs of TNFα-treated NIH 3T3 fibroblasts in the presence of cycloheximide. (**A**) Control cells, not incubated with TNF-α. Calibration bar: 2 μm. (**B**) One hour after incubation with TNF-α. Blebs arise from all points of the cell surface. Calibration bar: 2 μm. (**C**) Two hours after incubation with TNF-α. Chromatin has condensed into strands and is accumulating at the nuclear membrane. Calibration bar: 2 μm. (**D**) Three hours after incubation with TNF-α. This cell, with one bleb, is surrounded by cell detritus. Its mitochondria are swollen and the cristae disrupted (small arrows). Compacted chromatin has accumulated in large amounts at the nuclear membrane (see detail in I). Calibration bar: 2 μm. (**E**) Four hours after incubation with TNF-α. All the organelles are disrupted, and the general organization of the cytoplasm has broken down. Calibration bar: 2 μm. (**F**) Six hours after incubation with TNF-α. The cell lacks an integral cell membrane. Calibration bar: 2 μm. (**G**) Detail of a control cell. Loosely floccular chromatin is sparsely present in the nucleoplasm, and light accumulations are present at some points of the nuclear membrane. Calibration bar: 300 nm. (**H**) Detail of a cell 1 h after incubation with TNF-α. A thicker layer of condensed chromatin is present at most points of the nuclear membrane, sparing the nuclear pores (small arrow). Calibration bar: 300 nm. (**I**) Detail of the cell shown in **D**, 3 h after incubation with TNF-α. Thick layers of densely compacted chromatin coat the nuclear membrane, sometimes sparing nuclear pores (small arrow). Calibration bar: 300 nm

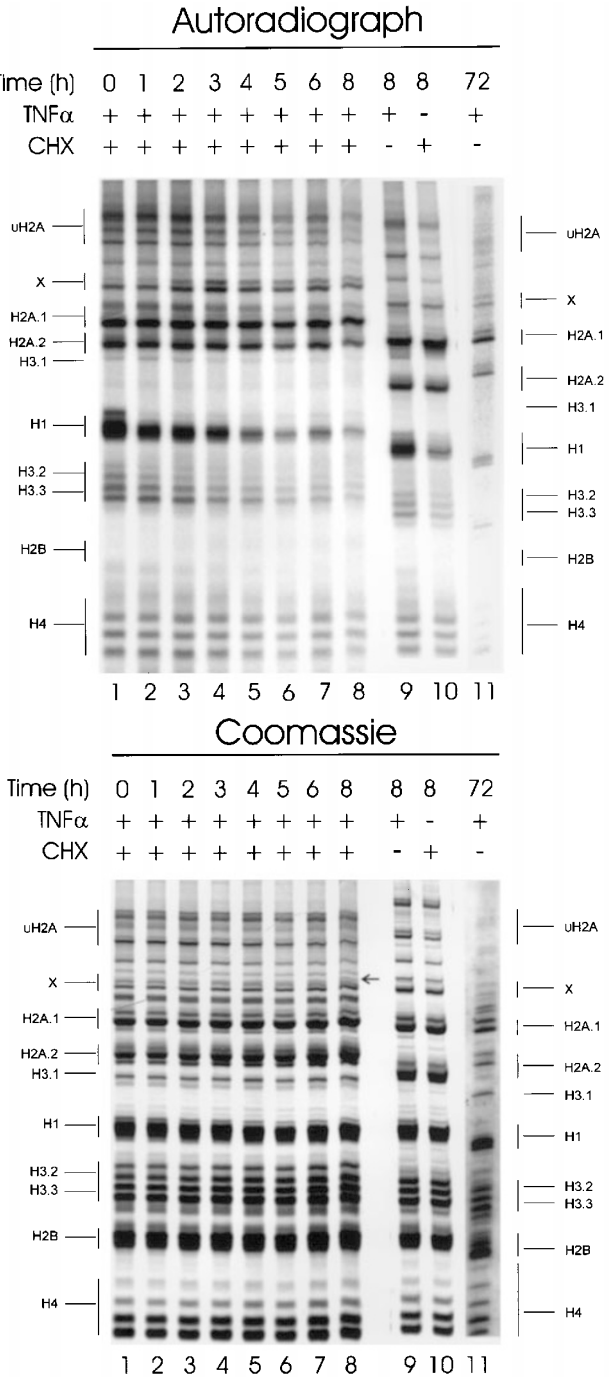

Figure 3 Incorporation of [^{32}P]orthophosphate into histones from apoptotic NIH 3T3 cells. The autoradiograph and the appropriate Coomassie-stained gel of histone variants separated on AUT–PAGE are shown. Lanes 1 to 8 represent histones from cells treated with TNFα in the presence of cycloheximide for 0, 1, 2, 3, 4, 5, 6 and 8 h, respectively. Lanes 9: histones of cells treated with TNFα alone for 8 h; lanes 10: histones of cells treated with cycloheximide alone for 8 h; lanes 11: histones of cells treated with TNFa alone for 72 h. The gel is a representative example of four independent experiments. Hyperphosphorylated histone variant marked X. Mass band of phosphorylated histone variant is marked with an arrow

with [^{32}P]orthophosphate at various time points for 60 min and after histone extraction AUT–PAGE in combination with autoradiography was used. It is obvious from the autoradiograph of Figure 3 that phosphate incorporation of nearly all histones continuously decreased substantially during the course of apoptosis, as compared to control cells (Figure 3, autoradiograph). This effect is very pronounced in H1 histones (decrease to 10% from control) but is also expressed in all H3 variants (decrease to 25% from control) and H4 histones (decrease to 50% from control) and to a lesser extent is also visible in H2A.1 and H2A.2 histones. Interestingly, ubiquitinated H2A histones which showed a considerable

phosphate incorporation at 0 h nearly completely stopped incorporation after 8 h of treatment. Neither TNFα nor cycloheximide alone was able to induce apoptosis after 8 h (Figure 3, lanes 9 and 10). They did not alter H2A.1 or H2A.2 phosphorylation, but diminished phosphate incorporation of H3, H4 and ubiquitinated H2A histones. Whereas TNFα treatment alone for 8 h does not influence H1 histone phosphate incorporation, cycloheximide nearly totally stopped H1 phosphorylation (Figure 3, lanes 9 and 10). In contrast to the dephosphorylation of most histones during the course of apoptosis, only two bands of histones showed a remarkable increase in phosphate incorporation (Figure 3, autoradiograph, marked X), which is paralleled by the appearance of a new band barely visible at 2 h after apoptosis induction (Figure 3, Coomassie, lane 3) but clearly detectable after 6 h and 8 h (Figure 3, Coomassie, lanes 7 and 8, arrow). The onset of phosphate incorporation at 2 h (threefold increase from control) with a maximum at 3 h (sixfold increase) and continuous incorporation for up to 8 h (twofold increase) (Figure 3, autoradiograph, lanes 3 to 8) was paralleled by the onset of chromatin condensation (Figure 2C, 2 h) and oligonucleosomal DNA laddering (Figure 1B, 2 h). Based on the results obtained with AUT gels we supposed that these two bands are phosphorylated H2A variants. Using TNFα or cycloheximide alone for 8 h, no increase in phosphorylation of the H2A variants was observed (Figure 3, autoradiograph, lanes 9 and 10). Interestingly, a 72-h treatment with TNFα in the absence of cycloheximide causing apoptosis in 65% of the cells was paralleled by an increase in H2A.X phosphorylation and a decrease in H1 phosphorylation (Figure 3, lanes 11).

SDS–PAGE and sequencing of phosphorylated H2A variants

To obtain more information about the identity of the bands shown in Figure 3, the core histones of cells treated for 8 h with cycloheximide alone or with the combination of TNFα and cycloheximide were subjected to SDS gel analysis (Figure 4A, lanes 1 and 2). In SDS gel H2A from cycloheximide-treated cells is the most prominent phosphorylated band in the core histone region (Figure 4A, lane 1). When cells were treated with cycloheximide plus TNFα, a second phosphorylated band was visible in the region of histone H3 or H2B on SDS gel (Figure 4A, lane 2). However, it was clearly visible on AUT gel (Figure 3) that H2B was not and H3 was only weakly phosphorylated during the 60 min of labeling. Since it is known that H2A.X migrates almost coincidentally with H2B or H3 in SDS gels, we conclude that the proteins in question are in fact phosphorylated forms of H2A.X. To definitively clarify this presumption, sequence analysis of the two proteins was performed. The labeled proteins were separated by reversed-phase HPLC (Figure 4B) and the resulting fractions designated 1 to 3 were analyzed on AUT–PAGE and autoradiographed. The autoradiograph of these separated fractions is shown in Figure 4C. Fractions 2 and 3 correspond to the two unknown phosphorylated bands. Because of the fact that the N terminus of histone H2A.X is blocked, the primary structure in that region was impossible to determine. We therefore digested the two fractions with endopeptidase GluC and separated the resulting peptides using reversed-phase HPLC (data not shown). Digestion of H2A.X with endopeptidase GluC, which cleaves at glutamic acid residues under the conditions applied, would be expected to yield a C-terminal fragment 49 residues long. In fact, we did detect such a C-terminal fragment in the two fractions, which was found to be radiolabeled. This C-terminal fragment was microsequenced and the first eight residues determined (bold letters) as 89**DEELNKLL**GGVTIA104 matching histone H2A.X. The specific activity of the upper phosphorylated band is twice as high as that of the lower phosphorylated H2A.X band, indicating that double the amount of phosphate was incorporated into each protein molecule in the upper band. Therefore, our experimental results indicate that the two labeled bands correspond to mono- and diphosphorylated histone H2A.X.

H1 subtype dephosphorylation pattern

In AUT–PAGE it was not possible to resolve H1 subtypes or to show single phosphorylated forms of H1 histones. Therefore, because H1 dephosphorylation is one of the most obvious events during the course of apoptosis (see Figure 3), we used reversed-phase HPLC and AUT–PAGE to prove whether a decrease in phosphate incorporation also leads to a decline in phosphorylated forms of the various H1 subtypes. Phosphate incorporation decreased quickly (Figure 5, autoradiograph, lane 2) during the early phase (1 h) of apoptosis to 50% from control (0 h). This extensive decline continued during the subsequent hours of treatment to 10% from control (Figure 5, autoradiograph, lanes 4 and 5), apparently causing the disappearance of phosphorylated forms of H1 subtypes (Figure 5, Coomassie, lanes 7 to 11). The main H1 subtypes of NIH 3T3 cells showed a considerable amount of phosphorylated forms in untreated cells: 55% of H1b, 45% H1c, 35% of H1d and H1e were phosphorylated forms in control cells, whereas 1 h after treatment the phosphorylated forms decreased of about 10%, 8 h after treatment only about 12% of H1b, 10% of H1c and 5% of H1d and H1e were phosphorylated. It must be emphasized, however, that treatment of cells with cycloheximide alone also tended to give nearly the same low level of phosphorylated H1 histones (see Figure 3, lanes 10 and Figure 5, lanes 6 and 12) without inducing typical apoptotic nuclear morphology during this time. Therefore, H1 dephosphorylation *per se* is clearly not able to induce chromatin condensation or DNA fragmentation but could be a prerequisite for chromatin alteration.

Phosphorylation changes in histone proteins after apoptosis induction with anti-Fas antibody or phosphatase inhibitor cantharidin

To determine whether phosphorylation events observed in TNFα-treated cells are comparable to the effect of other apoptosis inducers we examined the consequence of agonistic anti-Fas antibody or cantharidin treatment on these proteins. After 16 h of treatment with anti-Fas antibody in the presence of cycloheximide, 80% of the cells were apoptotic (Figure 6A, panel 1) and a DNA ladder was visible (Figure 6B, lane 1). Figure 7 shows that induction of Fas was able to trigger

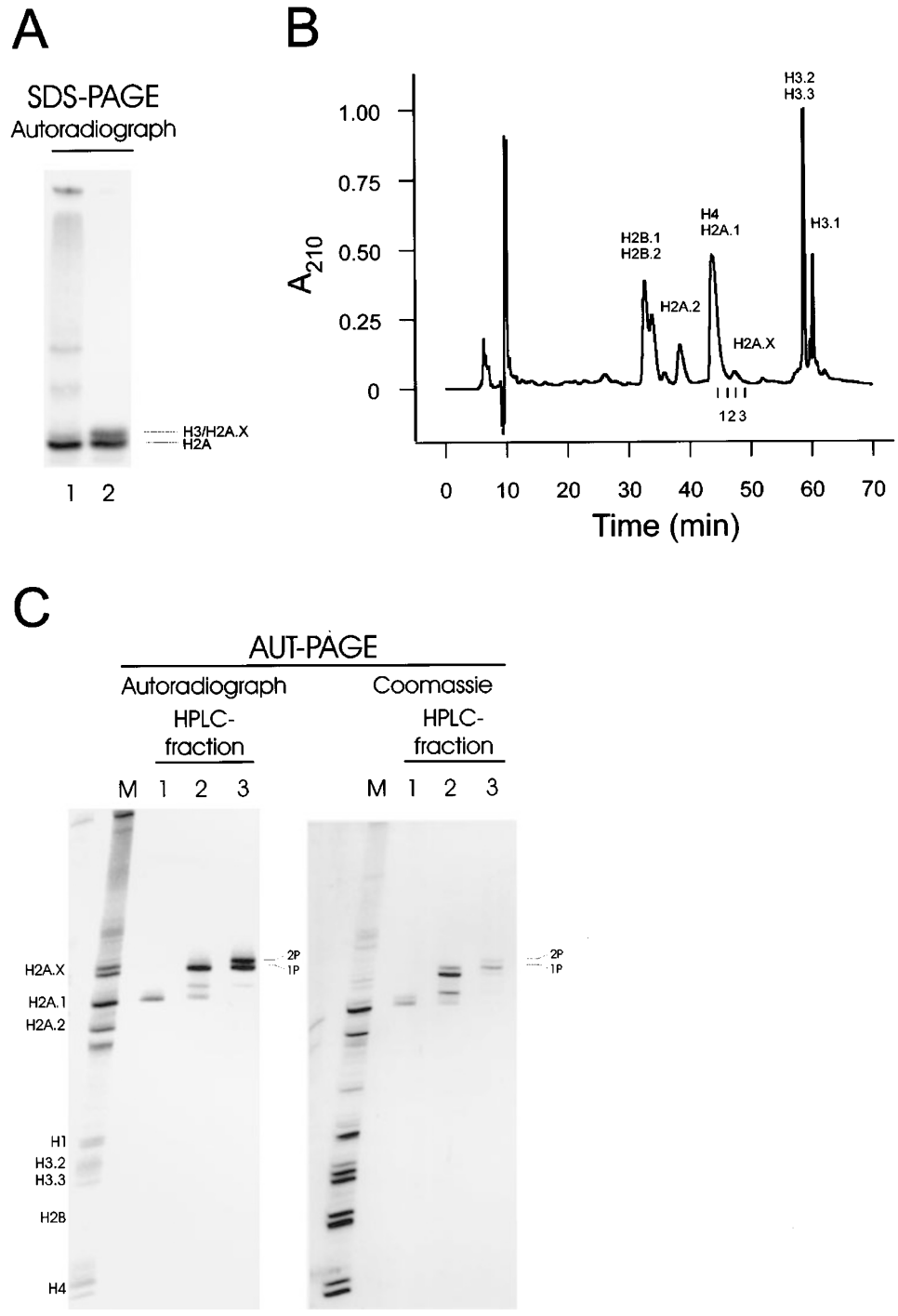

Figure 4 Characterization of [^{32}P]orthophosphate radiolabeled core histone H2A variant from apoptotic NIH 3T3 cells with SDS–PAGE, reversed-phase HPLC and AUT–PAGE. (**A**) Autoradiograph of histones separated on SDS–PAGE. Lane 1 : 8 h treatment with cycloheximide alone; lane 2 : 8 h treatment with TNFα in the presence of cycloheximide. (**B**) Reversed-phase HPLC was used to separate $^{32}PO_4$-radiolabeled core histones from apoptotic cells. Fractions 1 to 3 were collected for separation on AUT gels. (**C**) The fractions 1 to 3 from **B** were loaded on AUT–PAGE. After running and drying the gel, autoradiography was performed. Autoradiograph and Coomassie-stained gel of fractions 1 to 3 are shown. HPLC fraction 1: H2A.1; HPLC fraction 2: monophosphorylated H2A.X with traces of H2A.1; HPLC fraction 3: mono- and diphosphorylated H2A.X; M: basic nuclear proteins from apoptotic NIH 3T3 cells

hyperphosphorylation of H2A.X because, like in TNFα-treated cells (Figure 7, lanes 2 and 7), a diphosphorylated form of H2A.X (Figure 7, lanes 3 and 8, arrow 2) was visible in the autoradiograph. H1, H3 and ubiquitinated H2A histones are dephosphorylated (Figure 7, lane 3). It has been reported that inhibitors of protein phosphatase type 1 (PP-1) and type 2A (PP-2A) either inhibit[18] or induce apoptosis[19] in various cell lines. Microscopic examination showed that 16 h of canthar-

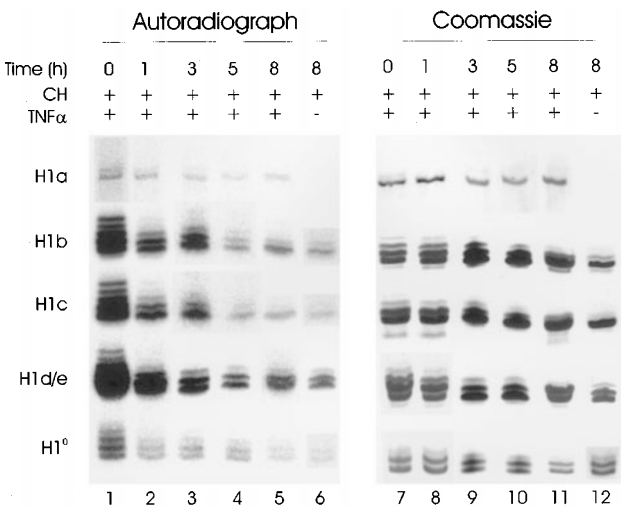

Figure 5 [^{32}P]orthophosphate incorporation of histone H1 subtypes in apoptotic NIH 3T3 cells. The H1 histones were separated in the first dimension with reversed-phase HPLC followed by AUT – PAGE as the second dimension. Autoradiograph and Coomassie-stained gel of phosphorylated H1 histone subtypes are shown. Lanes 1 to 5 (autoradiograph) and lanes 7 to 11 (Coomassie-stained gel) represent various H1 subtypes from cells treated with TNFα in the presence of cycloheximide for 0, 1, 3, 5 and 8 h, respectively. Lane 6 (autoradiograph) and lane 12 (Coomassie-stained gel): H1 histone variants of cells treated with cycloheximide alone. The gels are representative examples of three independent experiments

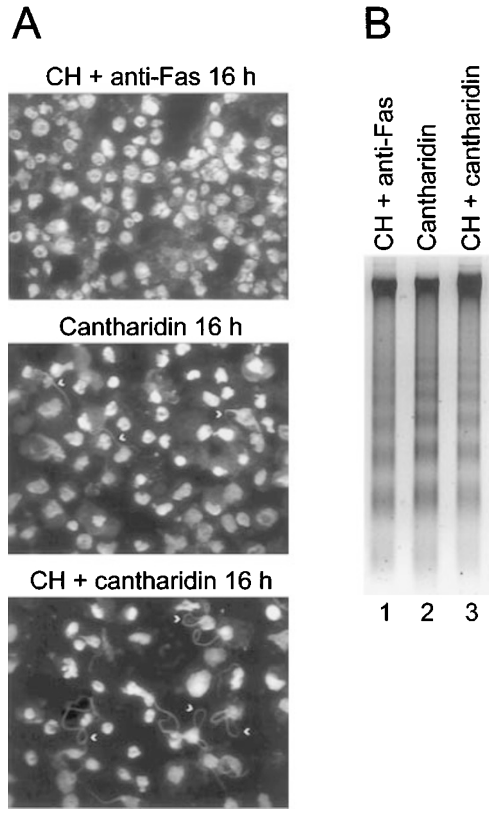

Figure 6 Apoptosis induction after treatment with anti-Fas antibody or protein phosphatase inhibitor 1/2A cantharidin. (**A**) Fluorescence microscopy of NIH 3T3 cells stained with Hoechst 33258. Panels (from top to bottom) correspond to 16 h anti-Fas antibody in the presence of cycloheximide (CH+anti-Fas 16 h), 16 h cantharidin, 16 h cantharidin in the presence of cycloheximide (CH+cantharidin 16 h). (**B**) DNA of apoptotic NIH 3T3 cells was separated on 2% agarose gel. Lanes 1 to 3 correspond to treatment with anti-Fas antibody in the presence of cycloheximide, cantharidin, cantharidin in the presence of cycloheximide, respectively

idin treatment caused apoptosis in around 80% of the NIH 3T3 cells (Figure 6A, panel 2), while DNA laddering was observable in agarose gel (Figure 6B, lane 2). Therefore, in cantharidin-treated cells not only condensation but also fragmentation of chromatin was induced. Interestingly, some of the cantharidin-treated cells showed chromatin fibers outside the nucleus (Figure 6A, panel 2, arrows). The phosphorylation pattern of cantharidin-treated cells (Figure 7, lanes 4 and 9) resembled that of TNFα- or anti-Fas antibody-treated cells in the presence of cycloheximide, because in H1 and ubiquitinated H2A histones only minimal phosphate incorporation occurred, whereas H2A.X was hyperphosphorylated. However, the hyperphosphorylation of H2A.X was more pronounced, because in addition to diphosphorylated H2A.X forms even triphosphorylated ones appeared (Figure 7, lanes 4 and 9, arrows 2 and 3). Furthermore, H3.2 and H3.3 histones were hyperphosphorylated as compared to those of mitotic cells, and also H2A.1 and H2A.2 showed an increase in phosphate incorporation and the appearance of a second phosphorylated form. It must be mentioned, however, that the triphosphorylated form of H2A.X and the diphosphorylated form of H2A.1 and H2A.2 can also be explained as a cantharidine-induced hyperacetylation of mono- or diphosphorylated H2A forms, also producing the observed banding pattern. The addition of cycloheximide to cantharidin-treated cells diminished the hyperphosphorylation of H3.2 and H3.3 histone variants but not that of histone H2A.X (Figure 7, lanes 5 and 10, arrows 2 and 3) and further decreased H1 phosphorylation. Microscopic examination of cantharidin plus cycloheximide-treated cells showed 80% of cells to have a typical apoptotic nuclear morphology; many of them showed chromatin fibers arranged in loops outside the nuclear membrane (Figure 6A, panel 3, arrows). DNA laddering was not more pronounced as compared to only cantharidin treatment (Figure 6B, lane 3). The Coomassie-stained AUT gels clearly demonstrated the mass amounts of the different phosphorylated forms of H2A.X. Whereas in control cells about 60% of unphosphorylated and 40% of monophosphorylated forms are present, TNFα- and Fas-treated cells show about 40% of unphosphorylated, 50% of monophosphorylated and 10% of diphosphorylated forms (Figure 7, Coomassie, lanes 6 to 8). In cantharidin-treated cells about 33% of unphosphorylated, 37% of monophosphorylated, 20% of diphosphorylated and 10% of triphosphorylated forms can be detected (Figure 7, Coomassie, lanes 9 and 10).

Effect of kinase inhibitors or activators on TNFα- or Fas-induced apoptosis and histone H2A.X phosphorylation

To obtain information concerning the kinase(s) responsible for apoptotic H2A.X phosphorylation *in vivo*, we induced apoptosis in the presence of specific kinase inhibitors or

activators (Table 1). Neither in TNFα- nor in Fas-treated cells did the simultaneous addition of PKC inhibitor staurosporine, tyrosin PK inhibitor genistein, PKA inhibitor H89, which at higher doses also inhibits PKG and PKC, or DNA PK inhibitor Wortmannin result in a marked specific suppression of the apoptosis inducer effects concerning cell morphology or H2A.X phosphorylation (Table 1). Whereas the MEK (MAP) kinase inhibitor PD98059 was not able to inhibit apoptosis, the MAP kinase activator and inhibitor of phosphatases 1 and 2A calyculin A induced by itself an apoptosis-like state comparable to that achieved with okadaic acid [20,21] or cantharidin. The PARP inhibitor 3-aminobenzamide, significantly delayed the TNFα induction of apoptosis but could not inhibit apoptosis or phosphorylation of H2A.X, whereas the protein kinase C activator PMA inhibited nearly completely induction of apoptosis and markedly reduced hyperphosphorylation of H2A.X but not dephosphorylation of H1 histones. In Fas-induced apoptosis none of the used kinase inhibitors or activators including PMA had an apoptosis-inhibiting effect or was able to prevent H2A.X hyperphosphorylation (Table 1) or H1 dephosphorylation.

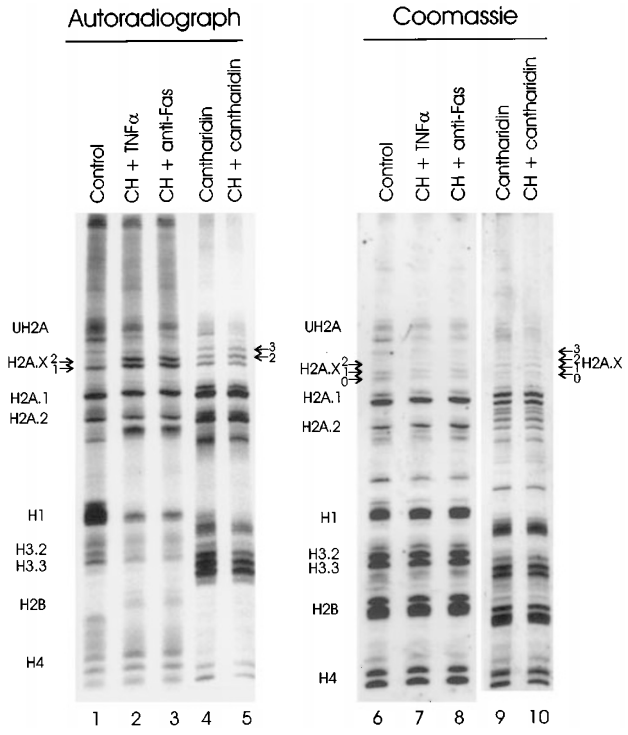

Figure 7 [^{32}P]orthophosphate incorporation of histone proteins after treatment with various apoptosis inducers. ^{32}P-radiolabeled basic nuclear proteins from apoptotic cells were separated on AUT–PAGE and autoradiography was performed. Autoradiograph and Coomassie-stained gel are shown: [^{32}P]orthophosphate incorporation of histones from untreated control cells (lanes 1 and 6), cells treated with TNFα in the presence of cycloheximide for 8 h (lanes 2 and 7), 16 h anti-Fas antibody-treated cells in the presence of cycloheximide (lanes 3 and 8), 16 h cantharidin-treated cells (lanes 4 and 9) or 16 h of cantharidin treatment in the presence of cycloheximide (lanes 5 and 10). Arrows with numbers indicate the phosphorylated forms of H2A.X; 1, 2 and 3 mean mono- di- or triphosphorylated forms

Effect of protease inhibitors on histone H2A.X phosphorylation of TNFα- or anti-Fas antibody-induced apoptosis

If H2A.X phosphorylation were directly correlated to apoptotic events, apoptosis inhibitors should be able to inhibit both TNFα- and Fas-induced apoptosis as well as the apoptosis-correlated hyperphosphorylation of histone H2A.X. The serine protease inhibitor TPCK (Figure 8A, lanes 5 and 12, and Figure 8B, lanes 5 and 10) had only a weak effect on apoptosis and H2A.X phosphorylation, whereas the caspase-1 inhibitor Ac-YVAD-cmk (Figure 8A, lanes 2 and 9, and Figure 8B, lanes 2 and 7) inhibited TNFα- but not anti-Fas antibody-induced apoptosis or H2A.X phosphorylation. The caspase-3 and caspase-7 inhibitor zDEVD-cmk was not able to inhibit apoptosis in TNFα-treated cells, and the phosphorylation pattern resembles that of apoptotic cells without caspase inhibtor (Figure 8A, lanes 6 and 13). The caspase inhibitor zVAD-(OMe)-fmk, which inhibits apoptosis at an early stage[22] (Figure 8A, lanes 3 and 10, and Figure 8B, lanes 3 and 8) and the nuclear scaffold proteinase inhibitor zAPF-cmk

Table 1 Kinase/phosphatase inhibitor/activator effects on H2A.X phosphorylation in TNFα- or anti-Fas antibody-induced apoptosis

	TNFα		Anti-Fas antibody	
Treatment	**H2A.X hyperphosphorylation**	**Apoptosis %**	**H2A.X hyperphosphorylation**	**Apoptosis %**
Untreated	–	2±1	–	2±1
Cycloheximide (5 μg/ml) alone	–	6±2	–	10±3
Without inhibitor	++	74±9	++	76±12
+H89, 2 μM	++	70±11	++	67±14
+Staurosporine, 10 nM	+	66±8	+	70±11
+Genistein, 100 μM	++	65±5	++	67±13
+PD98059, 10 μM	++	71±7	++	74±17
+Calyculin A, 10 nM	++	75±6	++	77±8
+3-aminobenzamide, 1 mM	+	55±22	++	75±11
+Wortmannin, 5 μM	++	72±11	++	78±7
+PMA, 150 nM	–	17±11	+	70±7

The number of apoptotic Hoechst 33258-stained cells with chromatin condensation and fragmentation was counted under a fluorescence microscope. ^{32}P-labeled H2A.X from apoptotic cells were run on AUT–PAGE. Autoradiography of ^{32}P-labeled proteins was conducted with PhosphorImager (Molecular Dynamics). The pixels of autoradiographic protein bands were counted and related to the pixels of the corresponding Coomassie blue-stained band with ImageQuant (Molecular Dynamics) and expressed as arbitrary units. H2A.X: –, less than 2; +, 2–5; ++, 10–20. The results represent the mean±S.D. of at least three independent experiments

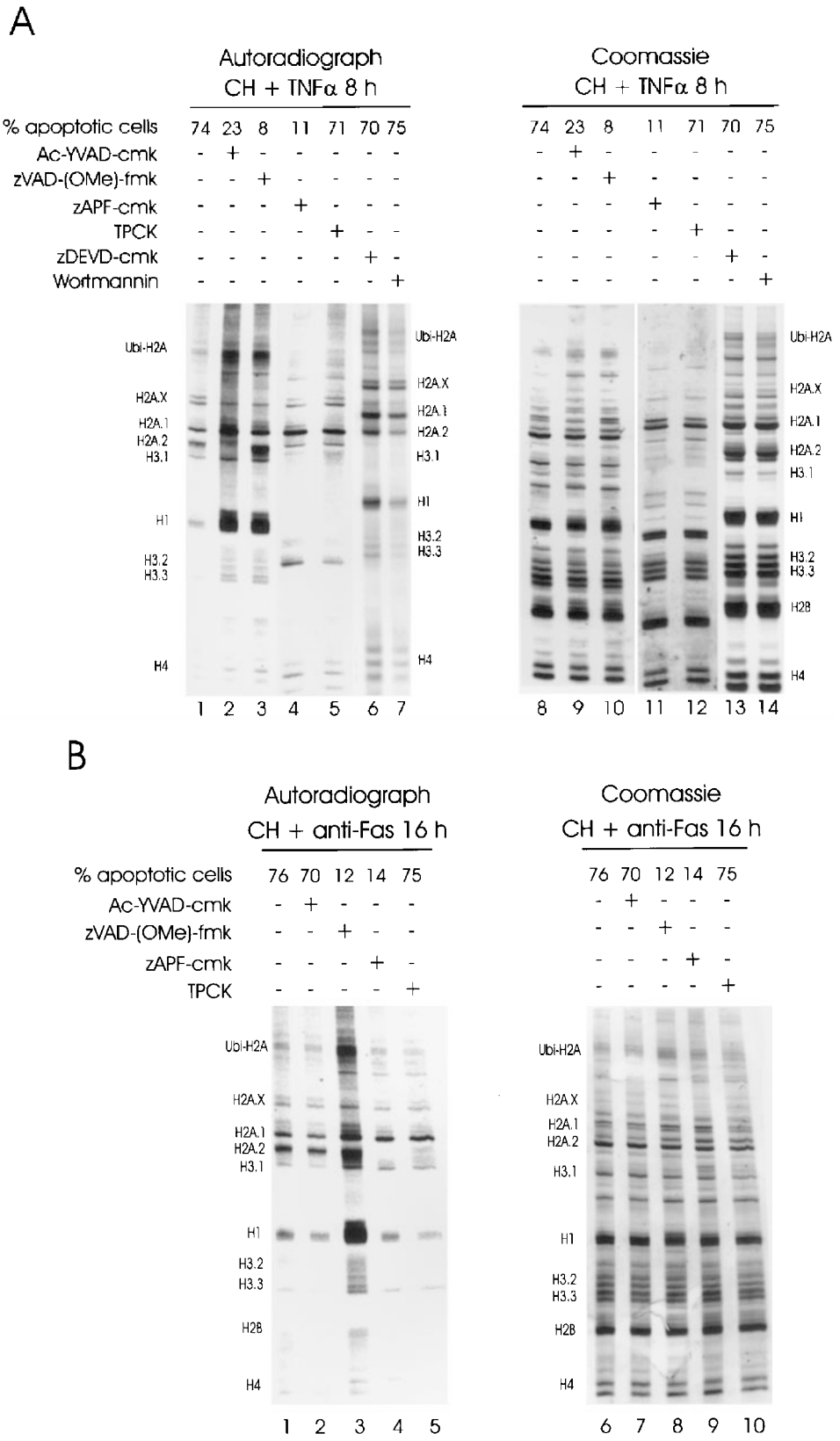

Figure 8 Effect of various proteinase inhibitors, caspase inhibitors and high concentration of DNA-PK inhibitor Wortmannin on apoptosis repression and histone H2A.X phosphorylation of TNFα- or Fas-treated cells. Autoradiographs of AUT–PAGE and the corresponding Coomassie-stained gels are shown. (**A**) Autoradiograph and Coomassie-stained gel of histones from cells treated 8 h with TNFα plus cycloheximide in the presence of the following inhibitors: lanes 1 and 8: without inhibitor; lanes 2 and 9: caspase-1 inhibitor Ac-YVAD-cmk (100 μM); lanes 3 and 10: caspase-8 inhibitor zVAD-(OMe)-fmk (100 μM); lanes 4 and 11:

(Figure 8A, lanes 4 and 11, and Figure 8B, lanes 4 and 9), however, nearly totally inhibited both apoptosis and H2A.X hyperphosphorylation. Moreover, dephosphorylation of histone H1 and ubiquitinated H2A was inhibited by Ac-YVAD-cmk and zVAD-(OMe)-fmk treatment in TNFα-induced apoptosis (Figure 8A, lanes 2, 3, 9 and 10) and by zVAD-(OMe)-cmk in anti-Fas antibody-treated cells (Figure 8B, lanes 3 and 8) but not by nuclear scaffold proteinase inhibitor zAPF-cmk. Therefore, histone H2A.X phosphorylation seems to be a downstream consequence of caspase(s) and nuclear scaffold proteinase(s), whereas the putative protein phosphatases or protein kinase inhibitors responsible for the dephosphorylation of H1 histones after apoptosis induction may be activated by a mechanism which acts downstream from the caspase-dependent activation of apoptosis at or near the apex of the apoptotic cascade but upstream from the nuclear scaffold proteinase.

Discussion

The aim of the study was to correlate the morphological changes occurring during development of apoptosis in NIH 3T3 cells to the major changes in phosphorylation status in histone proteins. Our report documents that phosphate incorporation of most histones, especially of all subtypes of H1 histones, decreased very rapidly after apoptosis induction with TNFα or anti-Fas antibody in the presence of cycloheximide. In the case of H1 histones we demonstrated that reduced phosphate incorporation evidently caused a strong reduction of phosphorylated forms of the main H1 histone subtypes in NIH 3T3 cells. Although phosphate incorporation in both H3 and H4 histones decreased after TNFα- or anti-Fas antibody-induced apoptosis, we were not able to detect a reduction of phosphorylated forms in AUT–PAGE. Furthermore, we also showed that phosphate incorporation and phosphorylated forms of ubiquitinated H2A histones decreased, which is consistent with the results of other laboratories.[23] During the course of apoptosis induced by TNFα or anti-Fas antibody, nearly no alteration of phosphorylated forms of H2A.1 or H2A.2 was detectable, whereas H2A.X became more highly phosphorylated with increasing amounts of diphosphorylated forms. In cantharidin-treated apoptotic cells H2A.X showed mono-, di- and even triphosphorylated forms, and H2A.1 and H2A.2 also became diphosphorylated.

Since the most pronounced changes in phosphate incorporation and mass pattern of phosphorylated forms apply to the H1 subtypes and histone H2A.X, and since these changes were found in apoptosis caused by all inducers we used, these histones were thought to most probably play a role in altering nuclear morphology.

Histone H2A.X belongs to the H2A subfamily, comprising about 10% of the H2A complement in NIH 3T3 cells, but shows differences as compared to H2A.1 and H2A.2. While the first 119 amino residues of the major histone H2A (H2A.1 and H2A.2) and H2A.X are homologous (96%), each histone has a unique carboxyl-terminal sequence.[24] Mouse H2A.X has an additional 13 amino acids at the carboxy terminus with the motif SQASQEY-(end) as compared to the other H2A histones.[25,26] The phosphorylation sites found by us were located on the C-terminal fragment (data not shown), which occurs after digestion with endopeptidase GluC. This part is on the exterior of the nucleosome and should be easily accessible to kinases.[27] Phosphorylated H2A.X has been suggested to play important roles in generation-spaced (180 bp) nucleosomal array.[28,29] Recently it was demonstrated[27,30] that on serine 139 H2A.X becomes phosphorylated rapidly and extensively after exposure of mammalian cell lines and mice to ionizing radiation, which leads to the formation of DNA double-stranded breaks. In a very recently published paper H2A.X phosphorylation was suggested to be closely linked to apoptotic DNA fragmentation as a DNA damage response prior to DNA repair.[31] Also in our present study we were able to demonstrate that during the course of apoptosis of NIH 3T3 cells the rise in phosphate incorporation into H2A.X and the increase in the diphosphorylated H2A.X form were obviously paralleled by the occurrence of internucleosomal DNA fragmentation (see Figures 1 and 3). Also, cantharidin-induced apoptosis prompted DNA fragmentation comparable to that induced by TNFα or anti-Fas antibody treatment. Histone H2A.X, however, was phosphorylated to a greater extent (mainly di- and triphosphorylated forms). In addition to a serine at position 1, where monophosphorylation occurs, mouse H2A.X contains two further serines at position 136 and 139.[27] The triphosphorylated form of H2A.X might be explained by these serines as the preferred substrates for the kinase. The fact that cantharidin treatment beside chromatin fragmentation and condensation also induced partial release of chromatin fibers was interpreted as histone hyperphosphorylation-induced decondensation of parts of the chromatin. It must be mentioned, however, that H2A.1, H2A.2 and H3 histones were also hyperphosphorylated in cantharidin-treated cells and might be responsible for this effect. Whether these findings are due to hyperphosphorylation or other factors like lamin or nuclear matrix degradation remains to be determined.

The decrease in phosphate incorporation and dephosphorylation of H1 histones occurred very rapidly during all treatments used in this study to induce apoptosis. One hour after commencing apoptosis induction with TNFα the amount of phosphorylated H1 histones was obviously diminished (see Figure 5). At this time a slight chromatin condensation at or near the nuclear membrane was also detectable in the electron micrograph (see Figures 2B and H) and only a shift in high molecular weight DNA but not in

nuclear scaffold proteinase inhibitor zAPF-cmk (50 μM); lanes 5 and 12: serine proteinase inhibitor TPCK (50 μM); lanes 6 and 13: caspase-3 and caspase-7 inhibitor zDEVD-cmk (200 μM); lanes 7 and 14: DNA-PK inhibitor Wortmannin (150 μM). (**B**) Autoradiograph and corresponding Coomassie-stained gel of histones from cells treated 16 h with anti-Fas antibody plus cycloheximide in the presence of the following inhibitors: lanes 1 and 6: without inhibitor; lanes 2 and 7: AC-YVAD-cmk (100 μM); lanes 3 and 8: zVAD-(OMe)-fmk (100 μM); lanes 4 and 9: zAPF-cmk (50 μM); lanes 5 and 10: TPCK (50 μM)

oligonucleosomal DNA was detected (see Figure 1B). H1 dephosphorylation was not inhibited by the PP1 and PP2A inhibitor calyculin A (data not shown). Moreover, the protein phosphatase inhibitor cantharidin by itself induced apoptosis, which is correlated to H1 dephosphorylation (see Figure 7, lanes 4 and 9). Therefore, a phosphatase other than PP1 or PP2A in combination with the inhibition of the putative H1 protein kinase of the CDK family must be responsible for the rapid dephosphorylation of H1 histones. The apoptosis-inducing ability of TNFα or anti-Fas antibody in the absence of cycloheximide was much slower (48 h to 72 h) than in the presence of cycloheximide (8 h to 16 h). A 72-h treatment with TNFα in the absence of cycloheximide causing apoptosis in 65% of the cells was clearly paralleled by an increase in H2A.X phosphorylation and a decrease in H1 phosphorylation. However, cycloheximide alone was not able to induce apoptosis during 16 h of treatment but also prompted H1 histone dephosphorylation (see Figures 3 and 5). Therefore, it can be concluded that, as expected, H1 dephosphorylation by itself is not able to induce apoptotic chromatin alterations, because rapid dephosphorylation of H1 histones also occurred during cell cycle after mitosis. Since H1 dephosphorylation preceded oligonucleosomal DNA fragmentation and paralleled chromatin condensation, we can speculate that chromatin alterations are accelerated and that H1 dephosphorylation makes DNA more accessible to DNase attack.

Our results exclude some of the kinases which could be responsible for phosphorylation of H2A.X. H2A.X is discussed as a substrate for phosphorylation by DNA-PK *in vitro*.[32] We used the PI3-K inhibitor Wortmannin in a concentration so high that it also works as a DNA-PK inhibitor.[33] Apoptotic NIH 3T3 cells, however, did not exhibit a noticeable deficit of highly phosphorylated H2A.X (see Figure 8, lanes 7 and 14), which prompted us to conclude that in the cell system used H2A.X is not the *in vivo* substrate of DNA-PK; this is in agreement with examinations of various DNA-PK-deficient mouse and hamster cell systems.[27] H2A.X may be involved in recognizing and repairing DNA strand breaks, but the phosphorylation of H2A.X seems to result from a DNA double-stranded break repair system that does not utilize DNA-PK.

The one or more kinases responsible for phosphorylation of H2A.X were influenced neither directly nor indirectly by protein kinase A[34] or G inhibitors, the tyrosine protein kinase inhibitor[35] or the MEK (MAP) kinase inhibitor used. Although the protein kinase C inhibitor staurosporine is described as inducing chromatin decondensation,[36] it was not able to inhibit chromatin condensation or fragmentation. Several reports show that the specific PARP inhibitor 3-aminobenzamide is able to inhibit cell death and apoptosis.[37] However, the ongoing apoptosis in NIH 3T3 cells after TNFα induction was only delayed and not inhibited. In this report we show that the phorbol ester PMA, a PKC activator, was able to inhibit TNFα-induced apoptosis together with phosphorylation of H2A.X, but only slightly influenced H1 dephosphorylation. It is known, however, that PKC activators inhibit receptor-mediated apoptosis[38] at a level upstream from caspase activation. Therefore the observed inhibition of H2A.X phosphorylation seems not to be directly linked to activation of PKC but could be a result of PKC-mediated inhibition of caspase activation. Activation of proteases and degradation of both the nuclear lamina and components of the intranuclear protein matrix enable aggregation of chromatin into apoptotic spherical bodies.[39] Furthermore, it is known that inhibition of lamin or nuclear scaffold degradation prevents nuclei from acquiring complete apoptotic features.[40, 41] Whereas hyperphosphorylation of H2A.X in apoptotic cells depends indirectly on activation of caspases and nuclear scaffold (lamin) proteases, as shown in zVAD-(OMe)-fmk or zAPF-cmk-treated cells, H1 dephosphorylation can be inhibited only by the caspase inhibitors zVAD-(OMe)-fmk and Ac-YVAD-cmk and not by the used nuclear scaffold protease inhibitor.

Materials and Methods

Cell culture and induction of apoptosis

NIH 3T3 fibroblasts were grown in monolayer cultures and cultivated in DMEM (Gibco LTD, Paisley, Scotland) supplemented with 10% fetal calf serum, penicillin (60 μg/ml) and streptomycin (100 μg/ml) in the presence of 5% CO_2. To induce apoptotic cell death cells were incubated with 100 ng/ml murine TNFα (Alexis Corporation, San Diego, USA) or 100 ng/ml anti-Fas antibody (JO2) (PharMingen, San Diego, USA) in combination with 2.5 μg/ml cycloheximide.

Protein kinase inhibitors and activators and proteinase inhibitors

We used H89 as protein kinase A and G inhibitor (2 μM), staurosporine as protein kinase C inhibitor (10 nM), phorbol 12-myristate 13-acetate as protein kinase C activator (150 nM), PD98059 as MEK (MAP) kinase inhibitor (10 μM), calyculin A as MAP kinase activator and phosphatase 1 and 2A inhibitor (10 nM), genistein as tyrosin protein kinase inhibitor (100 μM), and Wortmannin as DNA protein kinase inhibitor (5 μM and 150 μM). 3-aminobenzamide (1 mM) was used as poly(ADP-ribose) polymerase (PARP) inhibitor. Serine proteinase inhibitor Tos-Phe-chloromethylketone (TPCK) (50 μM), nuclear scaffold proteinase inhibitor Z-Ala-Pro-Phe-chloromethylketone (zAPF-cmk) (50 μM) or caspase inhibitors Ac-Tyr-Val-Ala-Asp-chloromethylketone (Ac-YVAD-cmk) (100 μM), Z-Asp-Glu-Val-Asp-chloromethylketone (zDEVD-cmk) (200 μM) and Z-Val-Ala-Asp(OMe)-fluoromethylketone (zVAD-(OMe)-fmk) (100 μM) were used for apoptosis inhibition. zAPF-cmk and the caspase inhibitors were from Bachem, Bubendorf, Switzerland. All other used substances were from Alexis Corporation, San Diego, USA.

Detection of apoptotic cells

Cell monolayers were incubated with TNF-α in the presence of cycloheximide, or left untreated as controls. Cells were harvested and resuspended in phosphate buffered normal saline (pH 7.4). One hundred microliters of cell suspension was fixed with 100 μl of 3% paraformaldehyde for 5 min at 4°C, washed with distilled water, dropped (10 μl) onto a slide and dried at room temperature. For inspection of chromatin, cells were stained with 8 μg/ml of Hoechst 33258. For electron microscopy the monolayers were

scraped off the substrate and the resulting cell suspensions fixed by addition of equal volumes of 5% glutaraldehyde in 100 mM cacodylate buffer (pH 7.4). Sixty minutes later the cells were pelleted by centrifugation at $200 \times g$ for 10 min, then fixed for a further 2 h in cacodylate-buffered 2.5% glutaraldehyde. Following two rinses in cacodylate buffer the cells were postfixed for 4 h in 2% osmium tetroxide, then dehydrated in graded alcohols, passed through acetone as intermedium and embedded in Epon. Ultrathin sections were cut, contrasted in uranium and lead salts, and viewed in a Zeiss EM10 electron microscope. For each specimen, approximately 100 cells were viewed and photographs made of individual cells representative of type commonly occurring in that specimen.

For the examination of DNA fragmentation cells treated with apoptosis inducer were lysed in 0.5 ml of a buffer containing 5 mM Tris, pH 8.0, 20 mM EDTA, and 0.5% (w/v) Triton X-100. After incubation for 15 min at 4°C, samples were centrifuged for 20 min at $15\,000 \times g$ to remove debris. The supernatant fraction containing fragmented DNA was digested with proteinase K (200 μg/ml) at 37°C for 3 h and then extracted once with an equal volume phenol followed by extraction with chloroform/isoamylalcohol (25/1). DNA was precipitated with 0.3 M sodium acetate and three volumes of ethanol at -70°C overnight. After centrifugation ($25\,000 \times g$) the precipitated DNA was washed with 95% ethanol and resuspended in a buffer containing 10 mM Tris, pH 8.0, 1 mM EDTA, and 50 μg/ml RNase A. After incubation at 37°C for 60 min, DNA was analyzed by 2% agarose gel electrophoresis.

Labeling conditions and isolation of H1 and core histones

For time course experiments NIH cells were labeled for 60 min in sodium phosphate-deficient DMEM with carrier-free [^{32}P]orthophosphate (1.2 mCi/2×10^7 cells per time point, 30 μCi/ml medium; NEN) during the various time points of treatment with TNFα. For all other experiments the cultures were incubated for 4 h. Thereafter, the labeling was stopped by washing with ice-cold PBS containing 50 mM $NaHSO_3$. For isolation of histones, nuclei from NIH fibroblasts were prepared as described.[13] H1 histones were isolated from the resulting nuclear preparations by extracting with 5% perchloric acid at 4°C for 1 h. The mixture was centrifuged at $10\,000 \times g$ for 20 min. The remaining pellet was resuspended with 0.4 M H_2SO_4 at 4°C for 1 h to extract the core histones. Thereafter, the mixture was centrifuged at $10\,000 \times g$ for 20 min. The H1 and core histones containing supernatants were mixed with trichloroacetic acid to the final concentration of 20% and allowed to stand for 1 h at 4°C. The precipitates were washed once with acetone-HCl and thereafter with acetone, resuspended in water containing 10 mM 2-mercaptoethanol, and freeze-dried.

RP-HPLC

The equipment used consisted of a 127 Solvent Module and a Model 166 u.v.-visible-region detector (Beckman Instruments, Palo Alto, CA, USA). The effluent was monitored at 210nm and the peaks were recorded using a Beckman System Gold software. Histone H1 separation was performed on a Nucleosil 300-5 C4 column (12.5 cm or 25 cm $\times$ 0.8 cm, 5 μ beads, 300 Å). The freeze-dried proteins were dissolved in 0.04 M 2-mercaptoethanol/water containing 0.1% TFA, and samples of 100 μg to 300 μg histones were loaded onto the column. At a constant flow rate of 1 ml/min and 1.5 ml/min the H1 histones were eluted using a 45-min linear gradient from 34–54% B (solvent A: water containing 15% ethylene glycolmonomethylether and 0.1% TFA, solvent B: ethylene glycolmonomethylether (15%)/70% acetonitrile (85%) with 0.1% TFA).[42–44]

Core histone separation was performed on a Ultrapore^{TM} C_3 column (25 cm $\times$ 1 cm I.D.; 5 μm particle pore size; 300 Å; end-capped; Beckman Instruments, Palo Alto, CA, USA). The lyophilized proteins were dissolved in 0.04 mM 2-mercaptoethanol/water containing 0.1% TFA, and samples of 500 μg were injected onto the column. At a constant flow of 1.5 ml/min the core histones were eluted using a two-step acetonitrile gradient starting at solvent A–solvent B (54 : 46) (solvent A: water containing 0.1% TFA; solvent B: 70% acetonitrile and 0.1% TFA). The concentration of solvent B was increased from 46% to 56% B during 45 min and from 56% to 100% B during 20 min. The protein fractions were collected and after adding 50 μl 2-mercaptoethanol (0.2 M) lyophilized and stored at -20°C.

The peptides obtained by digestion of histone H2A.X with Endoproteinase Glu-C were separated using a Nucleosil 300-5 C_{18} column (150 mm $\times$ 2 mm I.D.; 5 μm particle pore size; end-capped; Macherey-Nagel, Düren, Germany). Samples of $\sim$5 μg were injected onto the column. Chromatography was performed within 75 min at a constant flow of 0.3 ml/min with a two-step acetonitrile gradient starting at solvent A–solvent B (85 : 15) (solvent A: water containing 0.1% TFA; solvent B: 85% acetonitrile and 0.1% TFA). The concentration of solvent B was increased linearly from 15% to 60% during 60 min and from 60% to 100% during 15 min. Peptide fragments obtained in this way were analyzed by Edman degradation and ESI-MS.

Endoproteinase Glu-C digestion

Histone H2A.X ($\sim$5 μg) obtained by RP-HPLC fractionation was digested with Endoproteinase Glu-C from Staphylococcus aureus V8 (1/20 w/w) in 25 mM ammonium acetate buffer (pH 4.0) for 2 h at room temperature.

Gel electrophoresis and autoradiography

Histones were resolved both on SDS-18% polyacrylamide gel[45] and on 24-cm or 32-cm long Triton acid-urea-15% polyacrylamide gels (15% acrylamide, 0.125% bisacrylamide, 8 M urea, 6 mM Triton X-100, 5% acetic acid).[46,47] Gels were prerun for 6 h with a top layer of 1 mM cysteamine. Electrophoresis was carried out in 5% acetic acid, 0.1% (v/v) Triton X-100 with an applied constant current of 12 mA in a buffer-cooled electrophoresis tank for 18 h. Gels subsequently were fixed and stained with 0.1% Coomassie blue R 250. After staining and drying gels were quantified to estimate the protein quantities by using Hirschmann scanning densitometer and the Elscript 440 software. The radioactivity incorporated into each band was quantified by using Molecular Dynamics PhosphorImager and the ImageQuant software. The specific activity of each band was determined from the densitometric and PhosphorImager analysis.

Amino acid sequence analysis

Peptides were sequenced by Edman degradation on an Applied Biosystems model 492 pulsed-liquid protein sequencer equipped with an on-line model 120A HPLC analyzer. Typically, 5–50 pM of a peptide sample were run for 3–8 cycles as required for an unambiguous identification.

Acknowledgment

We are very grateful to A Devich, H Pirklbauer, J Forgo and Dr. M Rittinger for their excellent technical assistance.

References

1. Brown DG, Sun XM and Cohen GM (1993) Dexamethasone-induced apoptosis involves cleavage of DNA to large fragments prior to internucleosomal fragmentation. J. Biol. Chem. 268: 3037 – 3039
2. Wyllie AH, Kerr JF and Currie AR (1980) Cell death: the significance of apoptosis. Int. Rev. Cytol. 68: 251 – 306
3. Liu X, Zou H, Slaughter C and Wang X (1997) DFF, a heterodimeric protein that functions downstream of caspase-3 to trigger DNA fragmentation during apoptosis. Cell 89: 175 – 184
4. Enari M, Sakahira H, Yokoyama H, Okawa K, Iwamatsu A and Nagata S (1998) A caspase-activated DNase that degrades DNA during apoptosis, and its inhibitor ICAD. Nature 391: 43 – 50
5. Liu X, Li P, Widlak P, Zou H, Luo X, Garrard W and Wang X (1998) The 40-kDa subunit of DNA fragmentation factor induces DNA fragmentation and chromatin condensation during apoptosis. Proc. Natl. Acad. Sci. USA 95: 8461 – 8466
6. Takahashi A, Alnemri ES, Lazebnik YA, Fernandes-Alnemri T, Litwack G, Moir RD, Goldman RD, Poirier GG, Kaufmann SH and Earnshaw WC (1996) Cleavage of lamin A by Mch2α but not CPP-32: multiple interleukin 1β-converting enzyme-related proteases with distinct substrate recognition properties are active in apoptosis. Proc. Natl. Acad. Sci. USA 93: 8395 – 8400
7. Mashima T, Naito M, Noguchi K, Miller DK, Nicholson DW and Tsuruo T (1997) Actin cleavage by CPP32/apopain during the development of apoptosis. Oncogene 14: 1007 – 1012
8. Lazebnik YA, Kaufmann SH, Desnoyers S, Poirier GG and Earnshaw WC (1994) Cleavage of poly(ADP-ribose) polymerase by a proteinase with properties like ICE. (1994) Nature 371: 346 – 347
9. Martins LM and Earnshaw WC (1997) Apoptosis: alive and kicking in 1997. Trends Cell Biol. 7: 111 – 114
10. Han Z, Malik N, Carter T, Reeves WH, Wyche JH and Hendrickson EA (1996) DNA-dependent protein kinase is a target for a CPP32-like apoptotic protease. J. Biol. Chem. 271: 25035 – 25040
11. Ghayur T, Hugunin M, Talanian RV, Ratnofsky S, Quinlan C, Emoto Y, Pandey P, Datta R, Huang Y, Kharbanda S, Allen H, Kamen R, Wong W and Kufe D (1996) Proteolytic activation of protein kinase Cδ by an ICE/CED 3-like protease induces characteristics of apoptosis. J. Exp. Med. 184: 2399 – 2404
12. Bradbury EM (1992) Reversible histone modifications and the chromosome cell cycle. Bioessays 14: 9 – 16
13. Talasz H, Helliger W, Puschendorf B and Lindner H (1996) In vivo phosphorylation of histone H1 variants during the cell cycle. Biochemistry 35: 1761 – 1767
14. Wei Y, Yu L, Bowen J, Gorovsky MA and Allis CD (1999) Phosphorylation of histone H3 is required for proper chromosome condensation and segregation. Cell 97: 99 – 109
15. Sauve DM, Anderson HJ, Ray JM, James WM and Roberge M (1999) Phosphorylation-induced rearrangement of the histone H3 NH_2-terminal domain during mitotic chromosome condensation. J. Cell Biol. 145: 225 – 235
16. Ajiro K (2000) Histone H2B phosphorylation in mammalian apoptotic cells. An association with DNA fragmentation. J. Biol. Chem. 275: 439 – 443
17. Martin SJ, Reutelingsperger CP, McGahon AJ, Rader JA, Van-Schie RC, LaFace DM and Green DR (1995) Early redistribution of plasma membrane phosphatidylserine is a general feature of apoptosis regardless of the initiating stimulus: Inhibition by overexpression of Bcl-2 and Abl. J. Exp. Med. 182: 1545 – 1556
18. Song Q, Baxter GD, Kovacs EM, Findik D and Lavin MF (1992) Inhibition of apoptosis in human tumour cells by okadaic acid. J. Cell Physiol. 153: 550 – 556
19. Morimoto Y, Ohba T, Kobayashi S and Haneji T (1997) The protein phosphatase inhibitors okadaic acid and calyculin A induce apoptosis in human osteoblastic cells. Exp. Cell Res. 230: 181 – 186
20. Yamashita K, Yasuda H, Pines J, Yasumoto K, Nishitani H, Ohtsubo M, Hunter T, Sugimura T and Nishimoto T (1990) Okadaic acid, a potent inhibitor of type 1 and type 2A protein phosphatases, activates *cdc2*/H1 kinase and transiently induces a premature mitosis-like state in BHK21 cells. EMBO J. 9: 4331 – 4338
21. Ajiro K, Yoda K, Utsumi K and Nishikawa Y (1996) Alteration of cell cycle-dependent histone phosphorylation by okadaic acid. Induction of mitosis-specific H1 phosphorylation and chromatin condensation in mammalian interphase cells. J. Biol. Chem. 271: 13197 – 13201
22. Cohen GM (1997) Caspases: the executioners of apoptosis. Biochem. J. 326: 1 – 16
23. Marushige Y and Marushige K (1995) Disappearance of ubiquitinated histone H2A during chromatin condensation in TGFβ_1-induced apoptosis. Anticancer Res. 15: 267 – 272
24. West MH and Bonner WM (1983) Structural comparisons of mouse histones 2A.X and 2A.Z with 2A.1 and 2A.2. Comp. Biochem. Physiol. 76: 455 – 464
25. Gruber A, Streit A, Peist M, Benninger P, Boehni R and Schuemperli D (1990) Structure of mouse histone-encoding gene cluster. Gene 95: 303 – 304
26. Nagata T, Kato T, Morita T, Nozahi M, Kubota H, Yagi H and Matsushiro A (1991) Polyadenylated and 3′ processed mRNAs are transcribed from the mouse histone H2A.X gene. Nucleic Acids Res. 19: 2441 – 2447
27. Rogakou EP, Duane RP, Orr AH, Ivanova VS and Bonner WM (1998) DNA double-stranded breaks induce histone H2A.X phosphorylation on serine 139. J. Biol. Chem. 273: 5858 – 5868
28. Kleinschmidt JA and Steinbeisser H (1991) DNA-dependent phosphorylation of histone H2A.X during nucleosome assembly in Xenopus laevis oocytes: involvement of protein phosphorylation in nucleosome spacing. EMBO J. 10: 3043 – 3050
29. Dimitrov S, Dasso MC and Wolffe AP (1994) Remodeling sperm chromatin in Xenopus laevis egg extracts: the role of core histone phosphorylation and linker histone B4 in chromatin assembly. J. Cell Biol. 126: 591 – 601
30. Rogakou EP, Boon C, Redon C and Bonner WM (1999) Megabase chromatin domains involved in DNA double-strand breaks in vivo. J. Cell Biol. 146: 905 – 915
31. Rogakou EP, Nieves-Neira W, Boon C, Pommier Y and Bonner WM (2000) Initiation of DNA fragmentation during apoptosis induces phosphorylation of H2A.X histone at serine 139. J. Biol. Chem. 275: 9390 – 9395
32. Anderson CW (1993) DNA damage and the DNA-activated protein kinase. Trends Biochem. Sci. 18: 433 – 437
33. Christodoulopoulos G, Muller C, Salles B, Kazmi R and Panasci L (1998) Potentiation of chlorambucil cytotoxicity in B-cell chronic lymphocytic leukemia by inhibition of DNA-dependent protein kinase activity using wortmannin. Cancer Res. 58: 1789 – 1792
34. Waring P, Khan T and Sjaarda A (1997) Apoptosis induced by gliotoxin is preceded by phosphorylation of histone H3 and enhanced sensitivity of chromatin to nuclease digestion. J. Biol. Chem. 272: 17929 – 17936
35. Akiyama T, Ishida J, Nakagawa S, Ogawara H, Watanabe S, Itoh N, Shibuya M and Fukami Y (1987) Genistein, a specific inhibitor of tyrosine-specific protein kinase. J. Biol. Chem. 262: 5592 – 5595
36. Th'ng JPH, Guo XW, Swank RA, Crissman HA and Bradbury EM (1994) Inhibition of histone phosphorylation by staurosporine leads to chromosome decondensation. J. Biol. Chem. 269: 9568 – 9573
37. Malorni W, Rivabene R, Straface E, Rainaldi G, Monti D, Salvioli S, Cossarizzi A and Franceschi C (1995) 3-Aminobenzamide protects cells from UV-B-induced apoptosis by acting on cytoskeleton and substrate adhesion. Biochem. Biophys. Res. Commun. 207: 715 – 724
38. Masuda Y, Yoda M, Ohizumi H, Aiuchi T, Watabe M, Nakajo S and Nakaya K (1997) Activation of protein kinase C prevents induction of apoptosis by geranylgeraniol in human leukemia HL60 cells. Int. J. Cancer 71: 691 – 697
39. Hendzel MJ, Nishioka WK, Raymond Y, Allis CD, Bazett-Jones DP and Th'ng JPH (1998) Chromatin condensation is not associated with apoptosis. J. Biol. Chem. 273: 24470 – 24478
40. Lazebnik YA, Cole S, Cooke CA, Nelson WG and Earnshaw WC (1993) Nuclear events of apoptosis in vitro in cell-free mitotic extracts: a model system for analysis of the active phase of apoptosis. J. Cell Biol. 123: 7 – 22
41. Rao L, Perez D and White E (1996) Lamin proteolysis facilitates nuclear events during apoptosis. J. Cell Biol. 135: 1441 – 1455
42. Lindner H, Helliger W and Puschendorf B (1988) Separation of Friend erythroleukaemic cell histones and high-mobility-group proteins by reversed-phase high-performance liquid chromatography. J. Chromatogr. 450: 309 – 316
43. Lindner H and Helliger W (1990) Effects of eluent composition, ion-pair reagent and temperature on the separation of histones by high performance liquid chromatography. Chromatographia 30: 518 – 522

44. Talasz H, Sapojnikova N, Helliger W, Lindner H and Puschendorf B (1998) In vitro binding of H1 histone subtypes to nucleosomal organized mouse mammary tumor virus long terminal repeat promotor. J. Biol. Chem. 273: 32236 – 32243
45. Laemmli UK (1970) Cleavage of structural proteins during the assembly of the head of bacteriophage T4. Nature 227: 680 – 685
46. Bonner WM, West MHP and Stedman JD (1980) Two-dimensional gel analysis of histones in acid extracts of nuclei, cells, and tissues. Eur. J. Biochem. 19: 17 – 23
47. Zweidler A (1978) Resolution of histones by polyacrylamide gel electrophoresis in presence of nonionic detergents. Methods Cell Biol. 17: 223 – 233